Copper(I) oxide nanoparticle and tryptophan as its biological conjugate: A modulation of cytotoxic effects

ARTICLE *in* JOURNAL OF NANOPARTICLE RESEARCH · DECEMBER 2013

Impact Factor: 2.18 · DOI: 10.1007/s11051-013-2179-z

5 AUTHORS, INCLUDING:

Mritunjoy Maity
Indian Institute of Chemical Biology
4 PUBLICATIONS **2** CITATIONS
SEE PROFILE

Sumit kumar Pramanik
Hasselt University
13 PUBLICATIONS **29** CITATIONS
SEE PROFILE

Uttam Pal
Indian Institute of Chemical Biology
18 PUBLICATIONS **148** CITATIONS
SEE PROFILE

Nakul Maiti
Indian Institute of Chemical Biology
52 PUBLICATIONS **1,608** CITATIONS
SEE PROFILE

J Nanopart Res (2014) 16:2179
DOI 10.1007/s11051-013-2179-z

RESEARCH PAPER

Copper(I) oxide nanoparticle and tryptophan as its biological conjugate: a modulation of cytotoxic effects

Mritunjoy Maity · Sumit Kumar Pramanik · Uttam Pal · Biswadip Banerji · Nakul Chandra Maiti

Received: 28 March 2013 / Accepted: 26 November 2013

Abstract Recent investigations indicated that copper oxide nanoparticles can selectively induce apoptosis and effectively suppress the proliferation of tumor cells. Thus, it showed a great potential to be used as a drug for cancer treatment. Here we report an easy synthesis of spheroidal cuprous oxide nanoparticles (CuNPs) and their organic conjugate with L-tryptophan (Trp) using surfactant, sodium dodecyl sulfate as a capping reagent. The particles looked golden yellow and showed a strong affinity to bind blood carrier proteins such as bovine serum albumin and human serum albumin. However, both optical behavior and texture of the particles altered upon conjugation with Trp. The average size of the CuNPs was estimated to be ~70 nm as appeared under transmission electron microscope or atomic force microscope. The biological conjugate with Trp was ~85 nm and looked light sky blue in aqueous suspension. The surface of the conjugated nanoparticles was smoother than the bare CuNPs. The CuNPs were found to be toxic to different cultured cancerous cells; however, conjugation with Trp attenuated the toxicity, and indicated its possible utility in developing a drug candidate for cancer in a controlled fashion. Reduced toxicity also indicated a possible use of the conjugated particle as a drug delivery system.

Keywords Cuprous oxide · Nanoparticles · FT-IR · Fluorescence · Anticancer · Nanomedicine · Health effects

Introduction

Presently a considerable interest has been focused on studying the interaction of inorganic nanoparticles with organic and biological molecules and it is an exciting field of basic and applied research (Adleman et al. 2009; Hoffmann et al. 1995; Johnson 2003; Kamat 1993; Livage et al. 1988). Modification of inorganic nanoparticles with biological molecules, such as nucleic acids, peptides, and amino acids often found to modulate chemical and much optical behavior of nanoparticles (Chevrier et al. 2012). Evidences presented that nanoparticles coated with ligand could induce the response of receptors bound to the cell membranes without entering in the cell (Chen et al. 2008; Salata 2004). Engineered nanoparticles in suitable condition can also enter inside the cell after

Electronic supplementary material The online version of this article (doi:10.1007/s11051-013-2179-z) contains supplementary material, which is available to authorized users.

M. Maity · U. Pal · N. C. Maiti (✉)
Structural Biology and Bioinformatics Division, CSIR-Indian Institute of Chemical Biology, 4, Raja S.C. Mullick Road, Kolkata 700032, India
e-mail: ncmaiti@iicb.res.in

S. K. Pramanik · B. Banerji
Chemistry Division, CSIR-Indian Institute of Chemical Biology, 4, Raja S.C. Mullick Road, Kolkata 700032, India

Published online: 07 December 2013

binding to a receptor (Park et al. 2011; Salvati et al. 2013). Transferrin-coated gold nanoparticles proved to be internalized by HeLa cells into vesicles (Yang et al. 2005). Gold nanoparticles coated with alkaloids found to penetrate cell walls (Oskam 2006). Modification also affects the target specificity and toxic behavior of nanoparticles toward living cells (Nash et al. 2012; Salvati et al. 2013).

Apart from great use in optoelectronics, proper tailoring of nanoparticles showed ample potentials of the particles to be used in medicine as a drug carrier (Gelperina et al. 2005; Torchilin and Editor 2006) and cancer-cell imaging (Austin et al. 2011; Chen et al. 2011; Fan et al. 2012). Nanoparticles were found to influence the cellular function of cells and activity of enzymes (Wu et al. 2009) and in many cases it showed the strong toxic effect to living cells (Barillet et al. 2010; Chen et al. 2009; Hussain et al. 2005; Safi et al. 2011). Therefore, it requires target specificity and controlled toxicity to be useful in biomedical nanotechnologies (Choi et al. 2010; Yang et al. 2013). The study of the interaction of drug-conjugated gold nanoparticles with bovine serum albumin (BSA) has been reported (Joshi et al. 2011). For control and specific use functionalization of gold nanoparticles with amino acids (Ghosh et al. 2008; Lee et al. 2008; Wangoo et al. 2008), proteins and DNA were reported (Ravindra 2009; Rink et al. 2010). Studies also carried out to test how different metal oxide nanoparticles, for instances, ZnO and CuO nanoparticles could bind cellular component and the significance of the binding had been explained (Xu et al. 2012).

In the present manuscript, we report the synthesis and toxic behavior of cuprous oxide nanoparticles (CuNPs) and its conjugate with L-tryptophan (Trp) to tap the potential of cuprous oxide nanoparticles and use it in control way in treatment of cancer and other diseases. Cuprous oxide nanoparticles may possess properties similar to azurite minerals which often used in natural Chinese medicine and showed potential antitumor properties (Wang et al. 2012). Cuprous oxide nanoparticles also bind to the hydrosulfide group, similar to arsenic trioxide which is used as antitumor drugs and used to treat leukemia (Pelicano et al. 2006; Ramos and Aller 2008).

In cuprous oxide, copper is in an unstable oxidation state (I) with d^{10} electronic configuration similar to ZnO. ZnO nanoparticles showed selective toxicity toward leukemia cells (HL60) and the toxic effect was much less of peripheral blood mononuclear cells (Akhtar et al. 2012; Premanathan et al. 2011). Due to the similar d^{10} electronic configuration of cuprous oxide and zinc oxide, CuNPs may have a similar cytotoxic effect. Nanostructure of cuprous oxide, therefore, may have potential application in medicinal chemistry. We successfully synthesized such nanoparticle. Further, we prepared the conjugate of the cuprous oxide nanoparticles with Trp to modulate the toxic behavior of the nanostructure. Tryptophan is an essential amino acid and often found in many proteins as an interesting aromatic amino acid residue. Its acceptance to cellular system may have less toxic effect. The toxic behavior of both the CuNPs and its biological conjugate with Trp was measured using different cancerous cell lines. X-ray diffraction (XRD) and Fourier transform infrared (FT-IR) spectroscopic analysis were carried out to define the nanoentities and binding of tryptophan to CuNPs. Along with XRD, transmission electron microscope (TEM) and atomic force microscope (AFM) were used to characterize the topographic information of the produced particles. Optical properties of the materials were measured by UV–vis absorption spectroscopy. Binding analysis of the nanoparticles to BSA, human serum albumin (HSA) and lysozyme (Lys) were further carried out using the intrinsic fluorescence behavior of the proteins to test the binding abilities of the proteins to the nanoparticle.

Experimental

Materials

Copper(II) sulfate pentahydrate salt ($CuSO_4 \cdot 5H_2O$, 98 % pure), sodium dodecyl sulfate (SDS, 98 % pure), and NaOH (98 % pure) were purchased from Merck. L-Ascorbic acid (99 % pure) and Trp (>98 % pure) were purchased from Sigma-Aldrich. HPLC grade water and ethanol were purchased from Spectrochem (Mumbai, India). All of these chemicals were analytical grade and used as purchased without further purification.

Synthesis and characterization

Synthesis of cuprous oxide nanoparticles (CuNPs)

A simple and effective method was established to synthesize cuprous oxide nanoparticles using SDS as a

stabilizing agent, and the preparation was done at room temperature. A concentrated copper(II) sulfate pentahydrate salt, $CuSO_4 \cdot 5H_2O$ solution was made in deionised water (Milli-Q Millipore purified), and to this solution SDS solution was added under stirring condition. The optimized pH was 9.0, and the mole equivalent ratio of $CuSO_4 \cdot 5H_2O$ and SDS was established to be 1:6. The stirring continued for ~30 additional minutes until the solution color changed to pale blue from blue. In the next step, aqueous solution of ascorbic acid was added to the reaction mixture and the color became pale yellow. The stirring was continued for 10 additional minutes. The final concentrations of the reactants were 0.04, 0.24, and 0.16 M, respectively, of $CuSO_4 \cdot 5H_2O$, SDS and ascorbic acid. Finally, the pH of the solution was adjusted to 9.0 by slow addition of NaOH (0.5 M) solution under continuous and rapid stirring. The color of the solution quickly changed to golden/deep yellow indicating the appearance of the CuNPs. Stirring continued for additional 30 min. The yellow solution was centrifuged at 8,000 rpm to sediment CuNPs. The sedimented particles were dispersed in 99 % ethanol followed by centrifugation at 10,000 rpm for 10 min. This process was repeated thrice to remove excess SDS, ascorbic acid, and NaOH. The prepared nanoparticles appeared as golden yellow particles and the color was similar in the dry condition. Figure 1 shows the color photograph of CuNPs taken under fluorescent room light.

Preparation of CuNPs: L-tryptophan conjugate

Conjugation of Trp to CuNPs was made to modify the surface property and activity of the nanoparticle. CuNPs conjugate with Trp was made by mixing CuNPs solution in ethanol with an aqueous solution of Trp. The optimized weight percentage of CuNPs to Trp was 1:3.5. Briefly, 3 mg of purified CuNPs was dispersed in 10 ml ethanol (HPLC grade) using a water bath sonicator. Sonication results clear yellow solution of CuNPs. Subsequently, 10.5 mg Trp was dissolved in 20 ml water. These two solutions were mixed in a 50 ml round bottle flask and stirring continued for 1.5 h. The solution color changes from yellow to sky blue. The unbound tryptophan was separated by centrifugation at 10,000 rpm for 10 min. A solid appeared and it was further washed three times with HPLC grade ethanol and dried under vacuum.

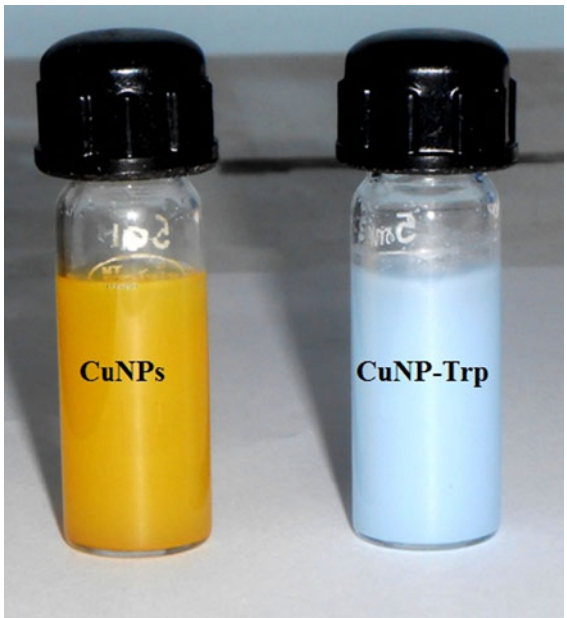

Fig. 1 Color photograph of aqueous suspension of CuNPs and its conjugate with Trp under room light (fluorescence lamp light). (Color figure online)

Photograph of the conjugate material is shown in Fig. 1 along with CuNPs.

Transmission electron microscopy

The size of the nanoparticles and their composite was studied using TEM. For TEM imaging, a drop of aqueous sample solution was placed on carbon-coated 300-mesh copper grid (Allied Scientific Product, USA) and dried in a dust free atmosphere. The bright field electron micrographs of the samples were taken on a Tecnai G2 Spirit Bio TWIN (Type: FP5018/40) at an acceleration voltage of 80 kV.

Atomic force microscope

AFM images were obtained on a Pico plus 5500 AFM (Agilent Technologies, Tempe, AZ, USA) with a piezo scanner, range of 9 μm. For the AFM imaging of CuNPs samples, 10 μl of the sample was deposited onto freshly cleaved muscovite Ruby mica sheets (ASTM V1 Grade Ruby Mica from MICAFAB, Chennai) for 5–10 min. The samples were washed gently with water and dried by nitrogen gas prior to AFM imaging. Micro-fabricated silicon cantilevers of 225 mm in length with a nominal spring force constant

of 21–98 Nm^{-1} were used from nanosensors. The cantilever oscillation frequency was tuned into the resonance frequency of 150–300 kHz. The images (512 × 512 pixels) were captured with a scan size of between 0.5 and 5 mm at a scan speed rate of 0.5 rpm. Images were processed by flattening, using Pico view software (Molecular Imaging Corporation, USA).

Fluorescence measurement

Intrinsic tryptophan fluorescence of BSA, HSA, and Lys was measured to investigate the binding of CuNPs to the protein molecules. All the fluorescence measurements were carried out using a Perkin Elmer LS-45 spectrofluorophotometer with a micromolar range protein concentration. Steady state fluorescence spectra were recorded with an excitation wavelength of 295 nm to selectively excite tryptophan residues in the protein molecules. The selected emission range was 310–450 nm. Both the excitation and emission slit widths kept at 2.5 nm. Most of the experiment was carried out at room temperature (25 °C).

For fluorescence quenching measurements, the intrinsic fluorescence of tryptophan residue(s) in the protein was measured in the presence and in the absence of CuNPs. The fluorescence of the protein was found to quench in the presence of CuNPs. The quenching experiment was carried out simply by adding 5 μl aliquot (stock solution each time) of concentrated (500 μM) CuNPs solution to 2 ml solution containing an appropriate concentration of HSA/BSA/Lys (2 μM in 20 mM sodium phosphate buffer, pH 6.5) taken in 1 cm path length quartz cuvette. Small error due to dilution upon addition of the CuNPs was neglected. CuNPs showed negligible absorbance at the excitation wavelength (295 nm) compared to protein absorption at this wavelength. Fluorescence intensities at 340 nm were recorded as a function of CuNPs concentration. To derive the binding parameters, obtained data were analyzed using modified Stern–Volmer (S–V) equation (Lakowicz 2006). Additional details are provided in the supplementary material.

Circular dichroism (CD)

The CD spectra were obtained at room temperature (25 °C) using a JASCO-810 spectropolarimeter under constant nitrogen flow condition. A 1 mm path length quartz cell was used for CD measurements and at room temperature. For all the measurement, the protein concentration of 10 μM was used. The far-UV region was scanned between 200 and 250 nm using bandwidth of 5 nm. Each represented spectra was average of five individual scans.

FT-IR experiment

The FT-IR spectra of the samples were recorded on a JASCO FT/IR 4200 spectrometer using the KBr disc technique. Solid samples were mixed with KBr in a clean glass pestle and mortar and compressed to obtain a pellet. The spectra were recorded from 400 to 4,000 cm^{-1}. Background spectra were obtained with a KBr pellet for each sample. JASCO software was used for data processing.

Cell culture preparation

Cytotoxicity tests were carried out using three cell lines: (i) human breast cancer cell line MCF 7, (ii) kidney cancer cell line HEK 293, and (iii) hepatocellular carcinoma cell line Hep G2. These cells were cultured in 25 cm^2 culture flasks using Dulbecco's modified Eagle's medium (DMEM, Invitrogen, Life Technologies, USA) supplemented with 10 % fetal bovine serum, 1 % nonessential amino acids, 1 % L-glutamine, and antibiotics (penicillin/streptomycin and gentamicin). The culture was maintained at 37 °C (CO_2 incubators) in an atmosphere of 5 % CO_2 and 95 % relative humidity. The growth medium was changed every alternate day until the time of the experiment. Prior to each cytotoxicity test, the cells were harvested by using trypsin, ethylenediamine tetraacetic acid (EDTA)-phosphate buffered saline (PBS) solution and diluted at a density of 6×10^5 cells/ml in MTT assay. The cell suspension was seeded in 96-well plate at 100 μl/well and incubated for about 24 h before the MTT test to reach the confluency.

The MTT assay

The MTT assay determines the ability of metabolically active viable cells to reduce the yellow tetrazolium salt [3-(4,5-dimethylthiazol-2-yl)-2,5-diphenyl tetrazolium bromide] (MTT, Mosmann 1983) to purple formazan crystals by mitochondrial dehydrogenase.

The concentration of purple color formazan crystals was spectrophotometrically (in ELISA reader) determined when dissolved in an organic solvent, dimethyl sulfoxide (DMSO). Cultured primary MCF 7, HEK 293, and Hep G2 were treated with tryptophan, CuNPs, and tryptophan-coated CuNPs separately (5, 10, 20, and 50 μM). The plates were incubated for 24 h at 37 °C in a humidified atmosphere of 5 % CO_2. MTT was dissolved in PBS at a concentration of 5 mg/ml, filtered through a 0.22 μm filter to sterilize and remove insoluble residues, and then stored in the amber vials at 4 °C. After treatment, the medium was removed and 50 μl of fresh medium was added along with 10 μl of MTT added in wells of the 96-well plates and incubated for 4 h at 37 °C in a humidified atmosphere of 5 % CO_2. At the end of the incubation period, the media were discarded using a suction pump. In a 96-well plates, 1.4 ml of DMSO was added to solubilize the purple crystals in different wells. The absorbance was measured at a test wavelength of 590 nm in an Elisa plate reader (Dynex MRX Microplate reader). The absorbance obtained from treated cells was expressed as percentages of absorbance obtained from untreated cells and is reported as mean ± SD ($n = 3$).

Results and discussion

Absorption spectroscopy

Figure 2**A** displays the UV–vis spectra recorded from the solution of CuNPs dispersed in aqueous solution at room temperature. It showed a wide band at ~470 nm. The band was due to plasma resonance excitation from the surface of the nanoparticles. The band position indicated the presence of cuprous oxide nanoparticle in the solution (Feng et al. 2012). The spectrum remained similar even after 90 min incubation at room temperature. It indicated the stability of the suspended particle. Under vacuum, the particles remained stable for months and the resuspended solution showed a similar spectrum (data not shown). The CuNPs were golden yellow in color; however, the composite (CuNP-Trp) became sky blue in aqueous solution (Fig. 1). This strongly indicated the formation of a composite with Trp. CuNP-Trp in water shows an absorption band similar to free tryptophan in aqueous solution (Fig. 2**B**). It confirmed the presence of Trp in the conjugate.

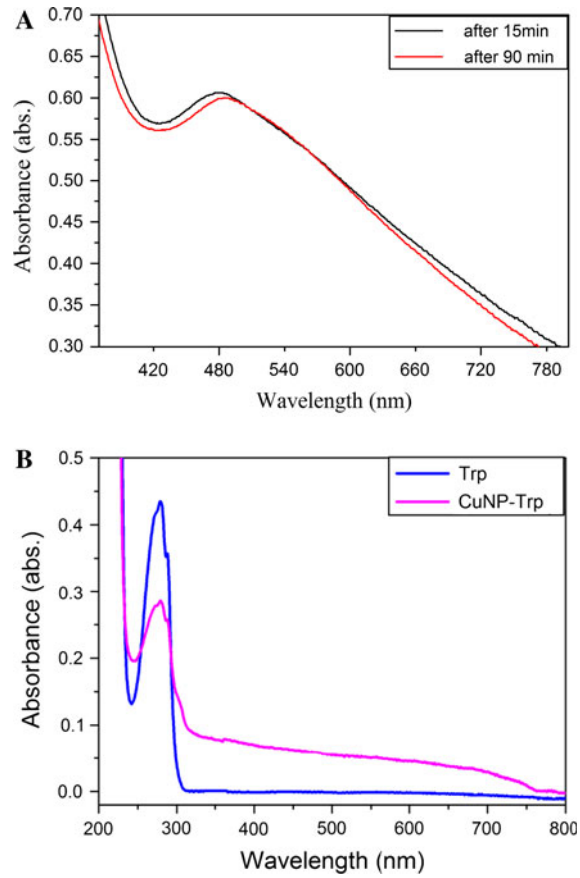

Fig. 2 **A** Optical spectra of CuNPs in deionised water. Deionised water was used as a reference. The time gap between the two readings was 75 min. **B** UV–vis spectrum of the 65 μM Trp (*blue*) and 20 μg/ml tryptophan-coated CuNPs (CuNP-Trp) (*pink*) in water suspension. Some broadness in the absorption spectrum of the CuNP-Trp was due to colloidal nature of the solution. (Color figure online)

X-ray diffraction study

Figure 3**A** shows the results of a XRD diffraction pattern of the CuNPs. The diffraction pattern of the particle was similar to cuprous oxide (Gou and Murphy 2003) and confirmed the formation of cuprous oxide nanoparticle. No strong peak from impurities was detected, it indicated that the major amount of particles were pure cuprous oxide. The XRD patterns showed peaks at $2\theta = 29.84$, 36.6, 42.46, 61.71, 73.93, and 77.52 which were indexed to (110), (111), (200), (220), (311), and (222) planes, respectively, of

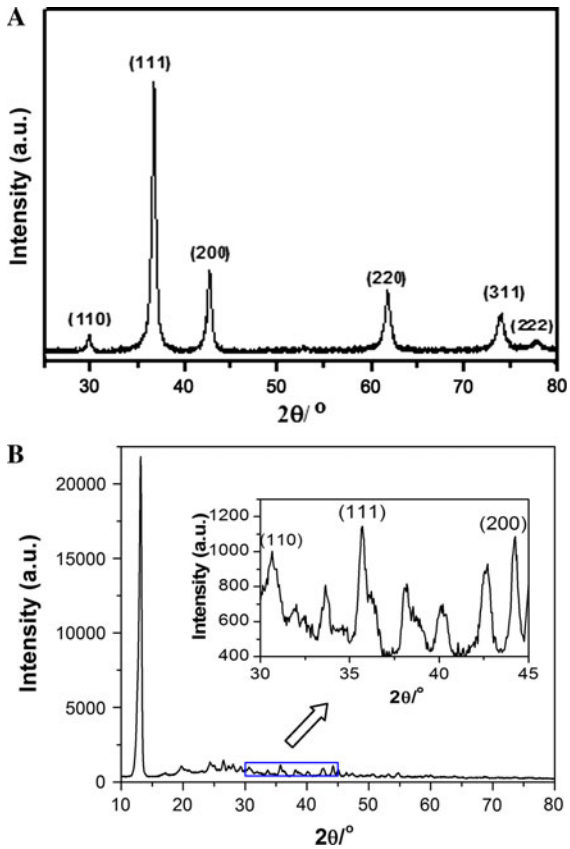

Fig. 3 **A** Powdered XRD pattern of the CuNPs. The peaks are labeled with the standard cuprite reflections. **B** Powder XRD pattern of CuNP-Trp. CuNP-Trp showed a strong peak due to the presence of aromatic ring of Trp residue. An expanded region in the *inset* shows the diffraction patterns of the nanoparticle

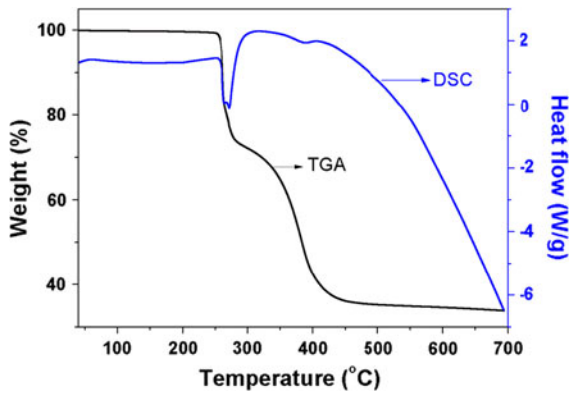

Fig. 4 Thermogravimetric analysis of Trp-conjugated Cu_2O nanoparticles

cubic cuprous CuNPs (JCPDS Card No. 05-0667). These XRD results matched well with cuprous oxide particles as reported by others (Gou and Murphy 2003; Kuo et al. 2007; Kuo and Huang 2008). XRD of the composite showed a very strong peak from the planer aromatic ring along with the signature peaks of the nanoparticle and confirmed the conjugation with Trp with the CuNPs (Fig. 3**B**).

Thermogravimetric and differential scanning calorimetric analysis

The thermal stability of the synthesized CuNP-Trp nanoparticles was monitored by thermo gravimetric analysis (TGA) and differential scanning calorimetric (DSC) analysis, and the thermogram is given in Fig. 4.

The experiment was carried out in SDT (simulated DSC and TGA) Q600 T.A. instrument. The tryptophan-conjugated CuNP (CuNP-Trp) was subjected to heating from 40 to 700 °C with a heating rate of 10 °C per min. TGA curve showed that the thermal decomposition process was represented by two step falls in weight over the temperature ranges from 250 to 295 °C and 310 to 475 °C. The weight loss between 250 and 295 °C was attributed to the dehydration of tryptophan, whereas the rest was due to the decomposition of organic content. The residual mass at 650 °C in the sample was 36 % and it indicated the high amount of a tryptophan contents in the tryptophan-coated Cu_2O nanoparticles.

Transmission electron microscopy

Topographic information of the nanoparticles and its conjugate was obtained from the TEM images taken at room temperature (24 °C). Figure 5 shows the TEM images of synthesized CuNPs and CuNP-Trp conjugate. The TEM pictures confirmed that the nanoparticles were well-dispersed, and the topography/morphology of the particles was spherical in nature. Some cases we observed particles in agglomerated state. Expanded image shows roughness of the surfaces and may be composed of smaller particles. In the TEM images the CuNPs appeared as a rough and of nonuniform spheroidal shape, however, the CuNP-Trp was smoother and spheroidal in shape.

Right side panel of respective TEM pictures in Fig. 5 shows the size distribution histogram of the nanoparticles with normal distribution fit. Histogram

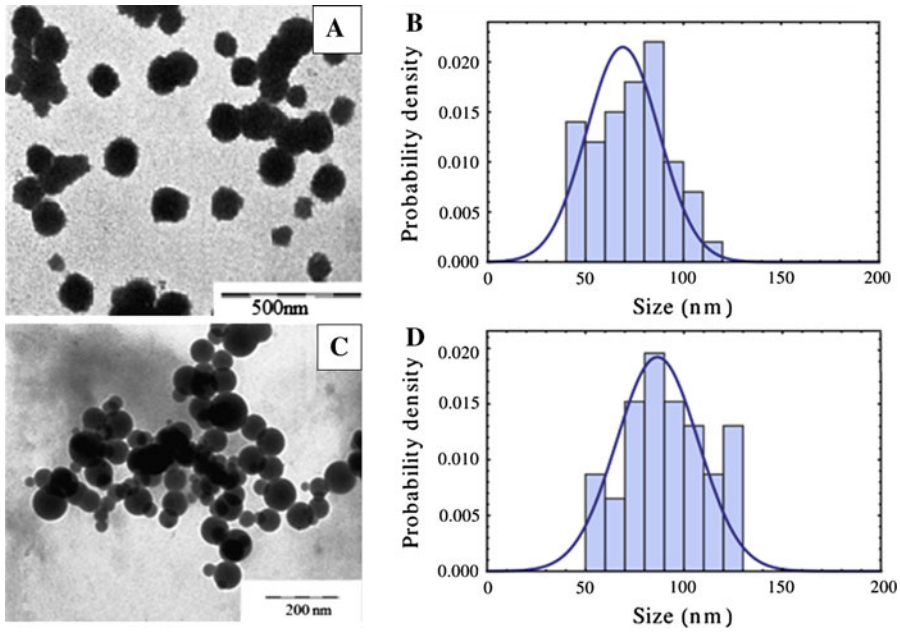

Fig. 5 Transmission electron microscopic (TEM) images of CuNPs (**A**) and its conjugate, CuNP-Trp (**C**). The size distribution histogram and the fitted normal distribution curve CuNPs (**B**) and CuNP-Trp (**D**) are shown beside the TEM images of respective samples

plot was made by measuring 100 randomly selected particles in enlarged TEM images. To determine the average particle size, the data were fitted with normal distribution function. The particle size of the CuNPs varied between 40 and 110 nm and the average diameter obtained was ~70 nm. The average particle size of CuNP-Trp nanocomposite was ~85 nm.

AFM studies

AFM image (two dimensional plot) of cuprous oxide nanoparticles and their conjugate with tryptophan is shown in Fig. 6, upper panels. Bottom panels showed the 3D-plot of the images and indicated length, width, and various height distributions. CuNPs were nearly spherical with 65–80 nm diameters. Nanoparticles conjugated with Trp also showed almost similar size distribution; however, density of larger particles was more than the numbers found in bare CuNPs. XRD analysis showed relatively smaller size of the nanoparticles compared to the values obtained from dynamic light scattering (DLS), TEM, and AFM measurements. DLS analysis indicated average diameter of 95 and 127 nm, respectively, for the CuNPs and its conjugate (supplementary material). Nanocrystals are combined to form nanoparticles. DLS provides hydrodynamic radius of these nanoparticles which are composed of nanocrystals. The particle size may be further increased due to agglomeration in solution state.

FT-IR spectroscopy

The conjugation of CuNPs to Trp was confirmed by FT-IR spectroscopy; it also established the nature (oxidation state) of the copper nanoparticle formed. FT-IR spectra taken with KBr pellets Trp, CuNPs, and the conjugated particle are shown in Fig. 7. Being an aromatic amino acid, Trp showed strong FT-IR bands (Fig. 7a) (Pavia 2009). N–H stretching band (due to the presence of 1 and 2° amine) was observed at 3,402 cm^{-1}. The bands at 1,453 and 1,412 cm^{-1} are assigned to aromatic C=C stretching; other bands also closely matched with the reported values. The FT-IR spectrum of CuNPs (Fig. 7b) displays an absorption peak at ~624 cm^{-1} and attributed to the Cu(I)–O vibration (Fan et al. 2006; Prakash et al. 2007). The spectrum also exhibited no strong FT-IR bands at ~588, ~534, and 480 cm^{-1} indicating that the compound was free of cupric oxide (Cu(II)–O)

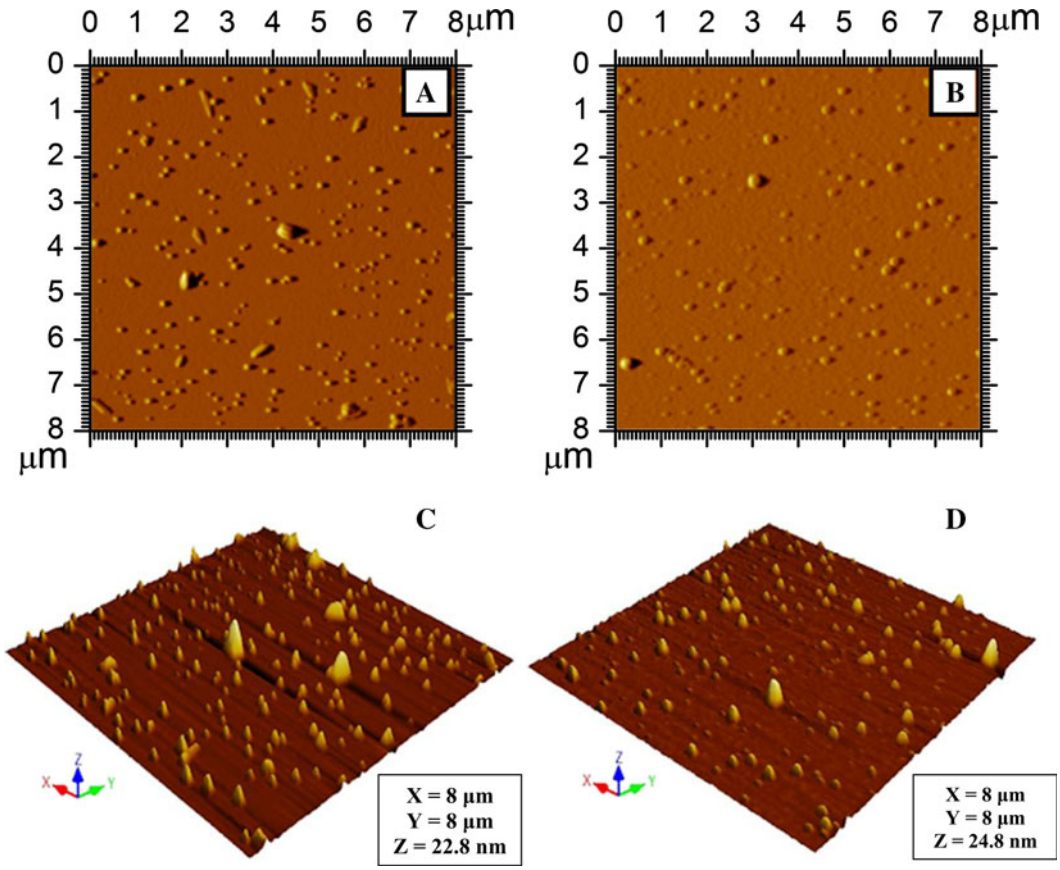

Fig. 6 AFM images of the nanoparticles. (**A**) and (**B**), respectively, are the topographic mode AFM images of CuNPs and CuNP-Trp. (**C**) and (**D**) show 3D-AFM images of CuNPs and CuNP-Trp, respectively. The area of each image is 8×8 µm^2. The particle size was estimated from the color density mapping

particles. FT-IR spectrum of CuNPs conjugated with Trp (Fig. 7c) showed many strong absorption bands due to incorporation of the tryptophan inside the nanoparticles. Expanded region also showed that the marker band for Cu(I)O was present and confirmed that the particles were preserved cuprous state. Tryptophan could bind CuNPs via its electron rich carboxylate group and the primary and secondary nitrogen atoms of the amino group. We observed overlapping N–H stretching bands for primary and secondary amines in free tryptophan at 3,402 cm^{-1}. However, in the composite their bands appeared at 3388, 3334, and 3271 cm^{-1}. It strongly suggested that the tryptophan nitrogen atoms are strongly interact with CuNPs and bound to it. The binding is possible through electropositive cuprous state via nitrogen atoms in the tryptophan ring, and COOH group also may be involved in the bonding.

Binding of the nanoparticles to BSA/HSA/lysozyme

Serum albumin proteins are often used as drug carrier in the blood. BSA, HSA, and Lys could bind many small molecules including drug candidates and carries to different cellular organs. We examined the binding affinity of the Cu_2O nanoparticles with blood carrier proteins, BSA, HSA, and also with hen egg white Lys. We utilized the intrinsic tryptophan fluorescence of individual proteins to determine the interaction behavior of CuNPs in aqueous solution. Figure 8 (upper panels) shows fluorescence spectra of individual proteins (BSA/HSA/Lys) in the absence and presence of different concentrations of CuNPs. The proteins showed a strong fluorescence with an emission peak at ~340 nm due to its tryptophan residue(s). The fluorescence intensity of proteins at ~340 nm

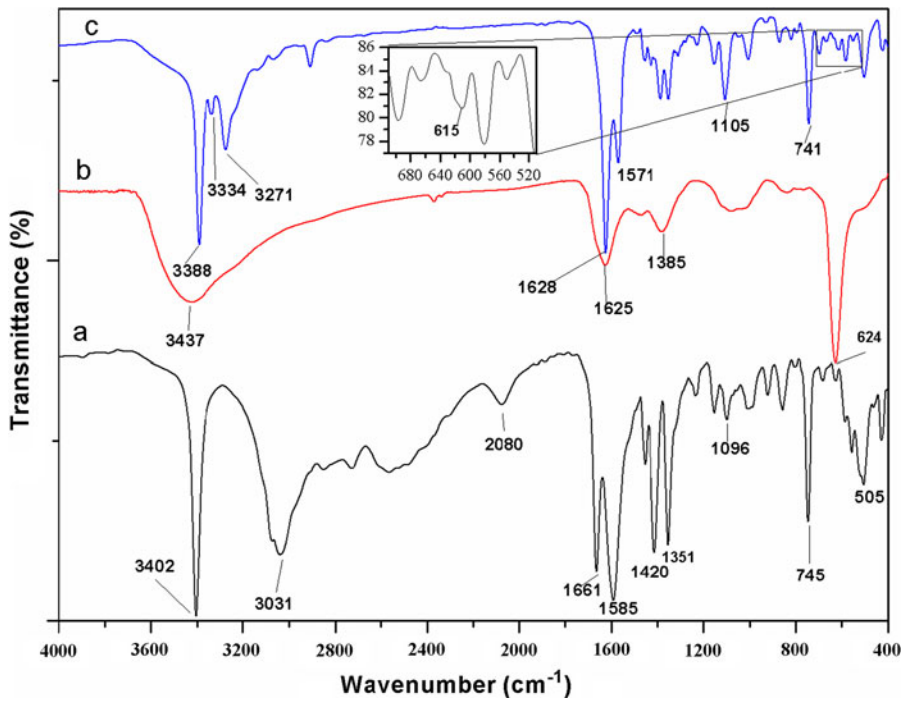

Fig. 7 FT-IR spectra of free tryptophan (a), CuNPs (b), CuNP-Trp (c) in solid state

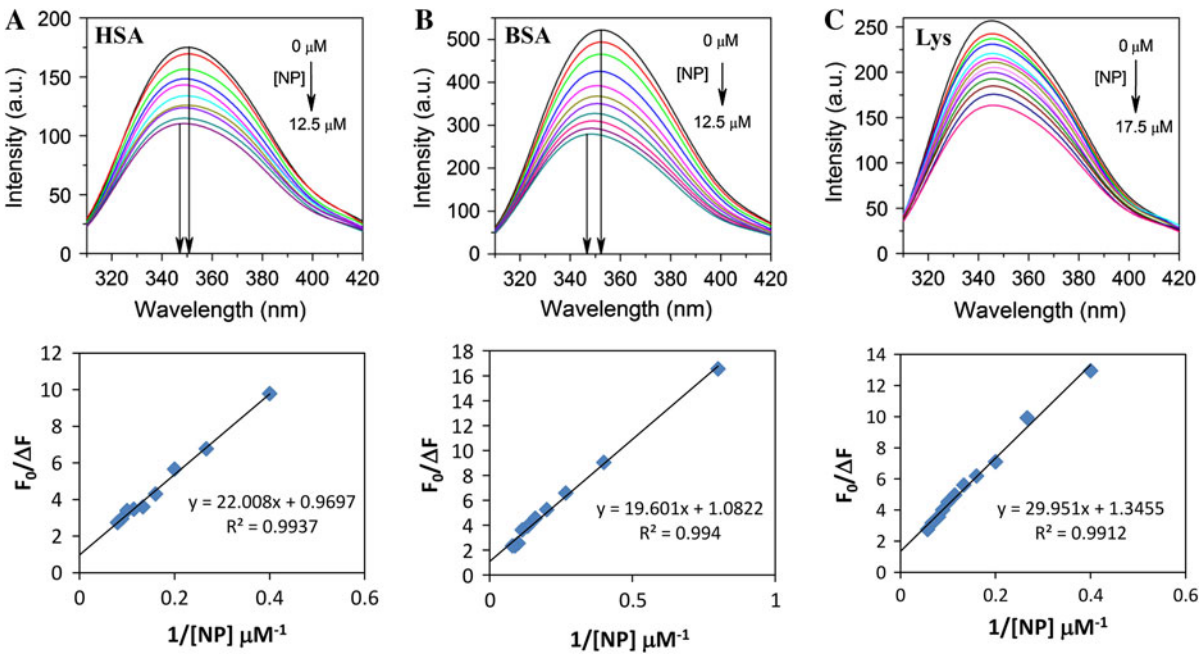

Fig. 8 Binding of CuNPs to BSA, HSA, and Lys assessed by intrinsic tryptophan fluorescence quenching. Fluorescence emission spectrum of 2.1 μM HSA (**A**), 2.4 μM of BSA (**B**), and 2.5 μM of Lys (**C**) in the presence and absence of CuNPs. Protein samples were prepared sodium phosphate buffer (20 mM), pH 6.5. Quenching was carried out with micromolar range (1.25–12.5 μM) CuNPs. $\lambda_{ex} = 295$ nm. The lower panel shows corresponding S–V plots obtained using the above fluorescence data

Table 1 Binding parameters (binding dissociation constant, K_d; binding affinity constant/S–V quenching constant, K_a)

	K_d (μM)	K_a (M^{-1})
HSA-NP	22.70	4.41×10^4
BSA-NP	18.10	5.50×10^4
LYS-NP	22.23	4.50×10^4

decreased gradually with increasing peptide concentration, indicating effective fluorescence quenching of the protein fluorescence.

To determine the binding behavior, the fluorescence data obtained in the above experiments were analyzed using a modified S–V equation (Eq. 1) (Lakowicz 2006, p. 289). Fluorescence peak intensity values of the protein at different concentration of CuNPs (Q) were used to fit a modified S–V equation as given below:

$$F_0/\Delta F = 1/(fK[Q]) + 1/f, \quad (1)$$

where F_0 is the initial fluorescence intensity in the absence of CuNPs, ΔF is the difference in fluorescence in the absence and presence of the CuNPs at concentration $[Q]$, K is the S–V quenching constant, and f is the fraction of the initial fluorescence which is accessible to the quencher (Lakowicz 2006). The plots of $F_0/\Delta F$ versus $1/[Q]$ yield f^{-1} as the intercept, and $(f\,\mathrm{K})^{-1}$ as the slope. Table 1 shows the result. The intercept on y axis ($1/f$) indicated that ~100 % of the total HSA fluorescence and ~90 % of BSA, ~74 % for Lys. Binding constant (K_d) was found to be in micro molar range, and the binding constants for HSA, BSA, and Lys quenching by CuNPs are given in Table 1. To derive the binding constant we used S–V quenching constants. Details are provided in supplementary materials.

Fluorescence quenching processes usually explained by two mechanisms: (i) dynamic fluorescence quenching and (ii) static quenching. Dynamic fluorescence quenching occurred either primarily via a collisional process, and solvent viscosity, and size of the particles play important roles on the extent of quenching. In static quenching process close association of the fluorophore and the quencher lead substantial decrease of fluorescence. Substantial fluorescence quenching of the protein by CuNPs indicated static fluorescence quenching and this static quenching arose from the formation of a (dark) complex between protein and CuNPs (Lakowicz 2006; Bian et al. 2004). The S–V quenching constant as obtained from the modified S–V equation can be expressed as binding affinity constant, K_a (Bian et al. 2004; Eftink and Ghiron 1976; Lakowicz 2006). Reciprocal of this K_a gives the dissociation constant, K_d (Table 1). See supporting material for detail analysis.

To determine the effect on protein conformation of CuNPs binding we carried out the CD as it often provides the secondary structures information of proteins in solution state. Different panels in Fig. 9 represent the CD spectra of BSA, HSA, and Lys in the presence and in the absence of CuNPs. Two negative bands that appeared appearing at ~208 and ~222 nm are the characteristics of α-helical conformation. The addition of the CuNPs into BSA, HSA, and Lys did not

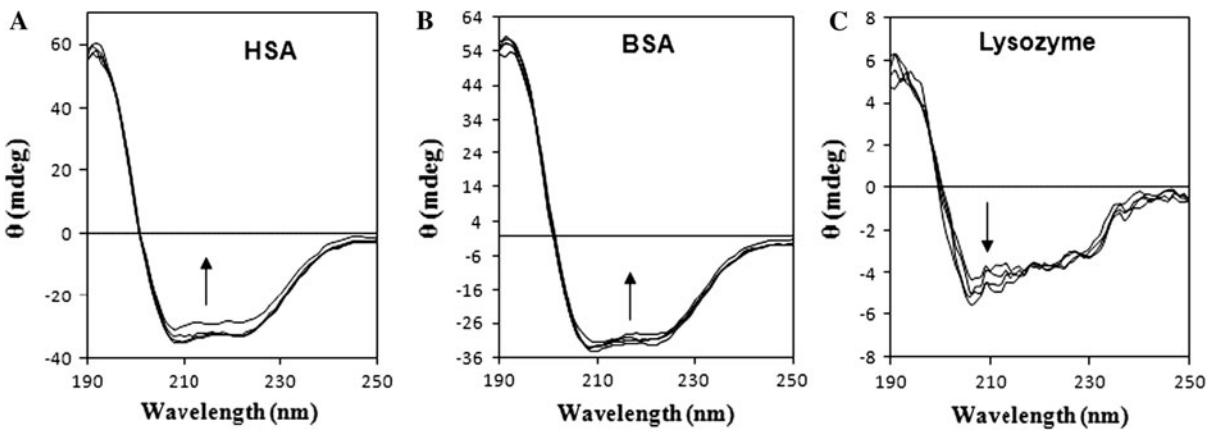

Fig. 9 Far-UV CD spectra of 2.0 μM of HSA (**A**), BSA (**B**) and Lys (**C**) in the absence and presence of CuNPs with concentration range of 0.0–25.0 μM. 2 μM. Protein samples were prepared in sodium phosphate buffer (20 mM), pH 6.5

cause huge perturbation of the CD spectrum indicating minor changes in the secondary structure of proteins when interact with the Cu_2O nanoparticles.

Cytotoxicity test

The in vitro cytotoxicity tests of the tryptophan, CuNPs nanoparticles, and tryptophan-coated CuNPs were performed with human breast cancer cell line MCF 7, kidney cancer cell line HEK 293, and hepatocellular carcinoma cell line Hep G2. Figure 10 shows the cell viability of these cancer cell lines after 24 h incubation of the control and with different concentrations of tryptophan, CuNPs, and tryptophan-coated CuNPs. It was observed that tryptophan did not induce any significant change in the proliferation with a concentration up to 50 μM with respect to the control, suggesting the absence of toxicity of the tryptophan. Subsequently the proliferation of MCF 7, HEK 293, and Hep G2 cells was reduced significantly with CuNPs which indicated the cytotoxic nature of the CuNPs. It was also noted that in all the concentrations the tryptophan-coated CuNPs; the cell viability was significantly increased and seemed to be less toxic toward MCF 7, HEK 293, and Hep G2 cell lines. This strongly indicated that incorporation/conjugation of Trp to CuNPs modified the chemical nature of the CuNPs and caused reduction in toxicity. The conjugate also showed dispersion stability in biological media (DMEM) (supplementary material).

The major aim of the current investigation was to test the cytotoxic effect of bare copper(I) oxide nanoparticles and its conjugate with Trp. Using different type of cultured cell lines, we showed that the cytotoxic effect was reduced when it was capped with Trp. Adsorption of tryptophan on nanoparticles found to provide smoothness to the surface, chemical nature got changed, and therefore, the interaction with other molecules such as proteins and others. It also produced sky blue color instead of dark yellow in water suspension (Fig. 1). It clearly indicated substantial effect on the electronic properties of the particle and resulted different interaction with the cell lines. The capping may prohibit the direct reaction of the cell surface and reduced the cytotoxic effect. It indicated possible dose-dependent utility in cancer therapy. Also, smoother surface and the lesser toxic effect put the CuNP-Trp conjugate as a viable drug carrier. Intrinsic copper(I) is unstable, very reactive, and toxic, and

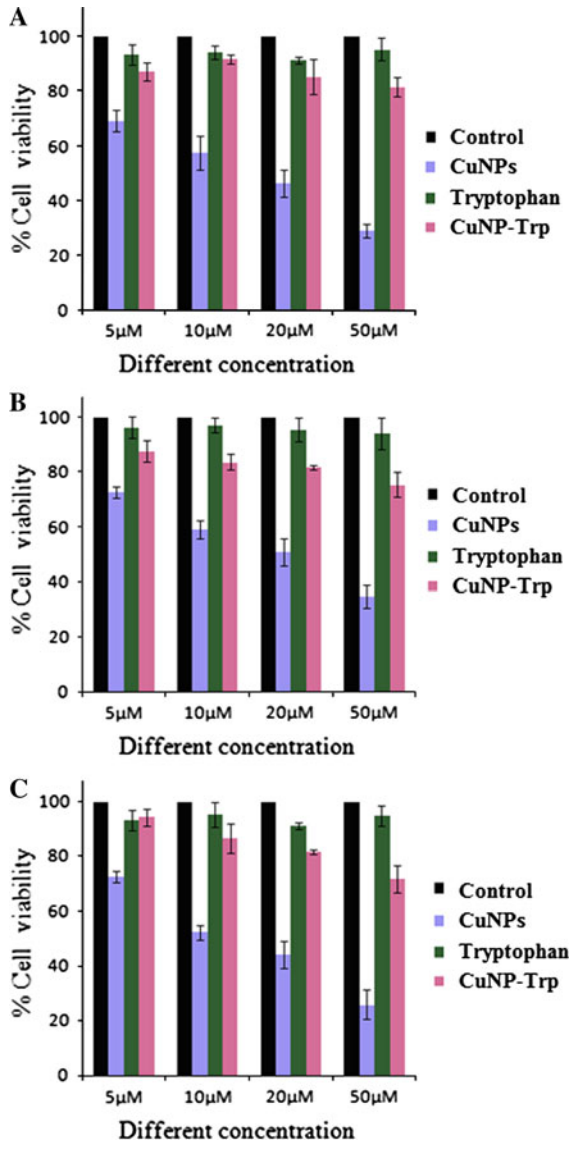

Fig. 10 Cytotoxicity of CuNPs on different cancer cell lines: MCF 7 (**A**), HEK 293 (**B**), HEP G2 (**C**) cell lines, respectively. Cells were treated with the CuNPs for 24 h

Cu(II) ion was not as toxic as its nanoparticles (Li et al. 2013; White et al. 1999). Due to the unstable nature of the ion, the cell viability test was not performed.

Conclusion

We reported here a successful synthesis of cuprous oxide nanoparticles at room temperature by reducing copper(II) sulfate with ascorbic acid in alkaline

condition. SDS served as the capping reagent during the preparation. Organic composite of the cuprous oxide nanoparticles was made with natural amino acid, Trp. Conjugation resulted new color, smoothness, and different texture and indicated its unique potential to be used in optoelectronics and material science. However, our interest oriented toward its possible application in medicinal science. The conjugated particles were less toxic toward cultured cells. The investigation also established that the CuNPs strongly bind to blood carrier protein molecules. These results indicated that CuNPs conjugated with Trp may have a potential role in medicinal chemistry and pathology. Dose-dependent use of the conjugate alone or with certain percentage of CuNPs may be beneficial for treatment of diseases. Another possibility as indicated earlier that it (CuNP-Trp) could be used as a drug carrier because of reduction in cytotoxic effect. An additional tailoring (making specific to particular receptor molecules) of the composite may be required to make it very target specific.

Acknowledgments Mritunjoy Maity thanks, Council of Scientific and Industrial Research (CSIR) for a fellowship (31/002(0897)/2011-EMR-I) and Uttam Pal thanks INSPIRE Fellowship Programme, Department of Science and Technology, Government of India, India. We gratefully acknowledge the grant support received from the miND (BSC0115), GENESIS (BSC0121), Structural Biology (BSC0113) projects of the Council of Scientific & Industrial Research and GAP-299 (Department of Biotechnology), Government of India. MM thanks to Mouni Roy for her comment on XRD data analysis and also thanks to Dr. (Mrs.) Aparna Laskar for TEM operation.

References

Adleman JR, Boyd DA, Goodwin DG, Psaltis D (2009) Heterogeneous catalysis mediated by plasmon heating. Nano Lett 9:4417–4423

Akhtar MJ, Ahamed M, Kumar S, Khan MAM, Ahmad J, Alrokayan SA (2012) Zinc oxide nanoparticles selectively induce apoptosis in human cancer cells through reactive oxygen species. Int J Nanomed 7:845–857

Austin LA, Kang B, Yen C-W, El-Sayed MA (2011) Plasmonic imaging of human oral cancer cell communities during programmed cell death by nuclear-targeting silver nanoparticles. J Am Chem Soc 133:17594–17597

Barillet S, Simon-Deckers A, Herlin-Boime N, Mayne-L'Hermite M, Reynaud C, Cassio D, Gouget B, Carriere M (2010) Toxicological consequences of TiO_2, SiC nanoparticles and multi-walled carbon nanotubes exposure in several mammalian cell types: an in vitro study. J Nanopart Res 12:61–73

Bian Q, Liu J, Tian J, Hu Z (2004) Binding of genistein to human serum albumin demonstrated using tryptophan fluorescence quenching. Int J Biol Macromol 34:333–337

Chen PC, Mwakwari SC, Oyelere AK (2008) Gold nanoparticles: from nanomedicine to nanosensing. Nanotechnol Sci Appl 1:45–66

Chen Y-S, Hung Y-C, Liau I, Huang GS (2009) Assessment of the in vivo toxicity of gold nanoparticles. Nanoscale Res Lett 4:858–864

Chen T, Shukoor MI, Wang R, Zhao Z, Yuan Q, Bamrungsap S, Xiong X, Tan W (2011) Smart multifunctional nanostructure for targeted cancer chemotherapy and magnetic resonance imaging. ACS Nano 5:7866–7873

Chevrier DM, Chatt A, Zhang P (2012) Properties and applications of protein-stabilized fluorescent gold nanoclusters: short review. J Nanophotonics 6:064504

Choi HS, Liu W, Liu F, Nasr K, Misra P, Bawendi MG, Frangioni JV (2010) Design considerations for tumor-targeted nanoparticles. Nat Nanotechnol 5:42–47

Eftink MR, Ghiron CA (1976) Fluorescence quenching of indole and model micelle systems. J Phys Chem 80:486–493

Fan C, Wang W, Zhao B, Zhang S, Miao J (2006) Chloroquine inhibits cell growth and induces cell death in A549 lung cancer cells. Bioorg Med Chem 14:3218–3222

Fan Z, Shelton M, Singh AK, Senapati D, Khan SA, Ray PC (2012) Multifunctional plasmonic shell-magnetic core nanoparticles for targeted diagnostics, isolation, and photothermal destruction of tumor cells. ACS Nano 6:1065–1073

Feng L, Zhang C, Gao G, Cui D (2012) Facile synthesis of hollow Cu_2O octahedral and spherical nanocrystals and their morphology-dependent photocatalytic properties. Nanoscale Res Lett 7:276

Gelperina S, Kisich K, Iseman MD, Heifets L (2005) The potential advantages of nanoparticle drug delivery systems in chemotherapy of tuberculosis. Am J Respir Crit Care Med 172:1487–1490

Ghosh PS, Kim C-K, Han G, Forbes NS, Rotello VM (2008) Efficient gene delivery vectors by tuning the surface charge density of amino acid-functionalized gold nanoparticles. ACS Nano 2:2213–2218

Gou L, Murphy CJ (2003) Solution-phase synthesis of Cu_2O nanocubes. Nano Lett 3:231–234

Hoffmann MR, Martin ST, Choi W, Bahnemann DW (1995) Environmental applications of semiconductor photocatalysis. Chem Rev 95:69–96

Hussain SM, Hess KL, Gearhart JM, Geiss KT, Schlager JJ (2005) In vitro toxicity of nanoparticles in BRL 3A rat liver cells. Toxicol In Vitro 19:975–983

Johnson BFG (2003) Nanoparticles in catalysis. Top Catal 24:147–159

Joshi P, Chakraborty S, Dey S, Shanker V, Ansari ZA, Singh SP, Chakrabarti P (2011) Binding of chloroquine-conjugated gold nanoparticles with bovine serum albumin. J Colloid Interface Sci 355:402–409

Kamat PV (1993) Photochemistry on nonreactive and reactive (semiconductor) surfaces. Chem Rev 93:267–300

Kuo C-H, Huang MH (2008) Facile synthesis of Cu_2O nanocrystals with systematic shape evolution from cubic to octahedral structures. J Phys Chem C 112:18355–18360

Kuo C-H, Chen C-H, Huang MH (2007) Seed-mediated synthesis of monodispersed Cu_2O nanocubes with five different size ranges from 40 to 420 nm. Adv Funct Mater 17:3773–3780

Lakowicz JR (2006) Principles of fluorescence spectroscopy, 3rd edn. Springer, New York

Lee SH, Bae KH, Kim SH, Lee KR, Park TG (2008) Amine-functionalized gold nanoparticles as non-cytotoxic and efficient intracellular siRNA delivery carriers. Int J Pharm 364:94–101

Li F, Lei C, Shen Q, Li L, Wang M, Guo M, Huang Y, Nie Z, Yao S (2013) Analysis of copper nanoparticles toxicity based on a stress-responsive bacterial biosensor array. Nanoscale 5:653–662

Livage J, Henry M, Sanchez C (1988) Sol–gel chemistry of transition metal oxides. Prog Solid State Chem 18:259–341

Mosmann T (1983) Rapid colorimetric assay for cellular growth and survival: application to proliferation and cytotoxicity assays. J Immunol Methods 65:55–63

Nash MA, Waitumbi JN, Hoffman AS, Yager P, Stayton PS (2012) Multiplexed enrichment and detection of malarial biomarkers using a stimuli-responsive iron oxide and gold nanoparticle reagent system. ACS Nano 6:6776–6785

Oskam G (2006) Metal oxide nanoparticles: synthesis, characterization and application. J Sol–Gel Sci Technol 37:161–164

Park J, Park J-H, Ock K-S, Ganbold E-O, Song N-W, Cho K-C, Lee S-Y, Joo S-W (2011) Preferential adsorption of fetal bovine serum on bare and aromatic thiol-functionalized gold surfaces in cell culture media. J Colloid Interface Sci 363:105–113

Pavia DL, Lampman GM, Kriz GS, Vyvyan JA (2009) Introduction to spectroscopy, 4th edn. Brooks/Cole Cengage Learning, Belmont

Pelicano H, Carew JS, McQueen TJ, Andreeff M, Plunkett W, Keating MJ, Huang P (2006) Targeting Hsp90 by 17-AAG in leukemia cells: mechanisms for synergistic and antagonistic drug combinations with arsenic trioxide and Ara-C. Leukemia 20:610–619

Prakash I, Muralidharan P, Nallamuthu N, Venkateswarlu M, Satyanarayana N (2007) Preparation and characterization of nanocrystallite size cuprous oxide. Mater Res Bull 42:1619–1624

Premanathan M, Karthikeyan K, Jeyasubramanian K, Manivannan G (2011) Selective toxicity of ZnO nanoparticles toward Gram-positive bacteria and cancer cells by apoptosis through lipid peroxidation. Nanomedicine 7:184–192

Ramos AM, Aller P (2008) Quercetin decreases intracellular GSH content and potentiates the apoptotic action of the antileukemic drug arsenic trioxide in human leukemia cell lines. Biochem Pharmacol 75:1912–1923

Ravindra P (2009) Protein-mediated synthesis of gold nanoparticles. Mater Sci Eng B 163:93–98

Rink JS, McMahon KM, Chen X, Mirkin CA, Thaxton CS, Kaufman DB (2010) Transfection of pancreatic islets using polyvalent DNA-functionalized gold nanoparticles. Surgery 148:335–345

Safi M, Yan M, Guedeau-Boudeville M-A, Conjeaud H, Garnier-Thibaud V, Boggetto N, Baeza-Squiban A, Niedergang F, Averbeck D, Berret J-F (2011) Interactions between magnetic nanowires and living cells: uptake, toxicity, and degradation. ACS Nano 5:5354–5364

Salata OV (2004) Applications of nanoparticles in biology and medicine. J Nanobiotechnol 2:1–6

Salvati A, Pitek AS, Monopoli MP, Prapainop K, Bombelli FB, Hristov DR, Kelly PM, Aberg C, Mahon E, Dawson KA (2013) Transferrin-functionalized nanoparticles lose their targeting capabilities when a biomolecule corona adsorbs on the surface. Nat Nanotechnol 8:137–143

Torchilin VP (ed) (2006) Nanoparticulates as drug carriers. Imperial College Press, London

Wang Y, Zi X-Y, Su J, Zhang H-X, Zhang X-R, Zhu H-Y, Li J-X, Yin M, Yang F, Hu Y-P (2012) Cuprous oxide nanoparticles selectively induce apoptosis of tumor cells. Int J Nanomed 7:2641–2652

Wangoo N, Bhasin KK, Mehta SK, Suri CR (2008) Synthesis and capping of water-dispersed gold nanoparticles by an amino acid: bioconjugation and binding studies. J Colloid Interface Sci 323:247–254

White AR, Multhaup G, Maher F, Bellingham S, Camakaris J, Zheng H, Bush AI, Beyreuther K, Masters CL, Cappai R (1999) The Alzheimer's disease amyloid precursor protein modulates copper-induced toxicity and oxidative stress in primary neuronal cultures. J Neurosci 19:9170–9179

Wu Z, Zhang B, Yan B (2009) Regulation of enzyme activity through interactions with nanoparticles. Int J Mol Sci 10:4198–4209

Xu M, Li J, Iwai H, Mei Q, Fujita D, Su H, Chen H, Hanagata N (2012) Formation of nano-bio-complex as nanomaterials dispersed in a biological solution for understanding nano-biological interactions. Sci Rep 2:406

Yang P-H, Sun X, Chiu J-F, Sun H, He Q-Y (2005) Transferrin-mediated gold nanoparticle cellular uptake. Bioconjugate Chem 16:494–496

Yang K, Feng L, Shi X, Liu Z (2013) Nano-graphene in biomedicine: theranostic applications. Chem Soc Rev 42: 530–547